Quadrupedal Locomotion With Parallel Compliance: E-Go Design, Modeling, and Control

Jiatao Ding, *Member, IEEE*, Perry Posthoorn, Vassil Atanassov, Fabio Boekel, Jens Kober, *Senior Member, IEEE*, and Cosimo Della Santina, *Senior Member, IEEE*

***Abstract*—To promote the research in compliant quadrupedal locomotion, especially with parallel elasticity, we present Delft E-Go, which is an easily accessible quadruped that combines the Unitree Go1 with open-source mechanical add-ons and control architecture. Implementing this novel system required a combination of technical work and scientific innovation. First, a dedicated parallel spring with adjustable rest length is designed to strengthen each actuated joint. Then, a novel 3-D dual spring-loaded inverted pendulum model is proposed to characterize the compliant locomotion dynamics, decoupling the actuation with parallel compliance. Based on this template model, trajectory optimization is employed to generate optimal explosive motion without requiring reference defined in advance. To complete the system, a torque controller with anticipatory compensation is adopted for motion tracking. Extensive hardware experiments in multiple scenarios, such as trotting across uneven terrains, efficient walking, and explosive pronking, demonstrate the system's reliability, energy benefits of parallel compliance, and enhanced locomotion capability. Particularly, we demonstrate for the first time the controlled pronking of a quadruped with asymmetric legs.**

***Index Terms*—Anticipatory control, parallel elastic actuation, quadrupedal robot, trajectory optimization.**

Manuscript received 20 January 2024; revised 31 March 2024; accepted 15 May 2024. Date of publication 5 June 2024; date of current version 16 August 2024. Recommended by Technical Editor H. Fathy and Senior Editor Q. Zou. This work was supported by the EU Project 101016970 NI. *(Corresponding author: Jiatao Ding.)*

Jiatao Ding, Fabio Boekel, and Jens Kober are with the Cognitive Robotics, Delft University of Technology, 2628 CD Delft, The Netherlands (e-mail: j.ding-2@tudelft.nl; f.g.m.boekel@student.tudelft.nl; j.kober@tudelft.nl).

Perry Posthoorn is with the DEMO, Delft University of Technology, 2628 CD Delft, The Netherlands (e-mail: p.posthoorn@tudelft.nl).

Vassil Atanassov is with the Department of Engineering Science, University of Oxford, OX1 3PJ Oxford, U.K. (e-mail: vassilatanassov@robots.ox.ac.uk).

Cosimo Della Santina is with the Cognitive Robotics, Delft University of Technology, 2628 CD Delft, The Netherlands, and also with the Institute of Robotics and Mechatronics, German Aerospace Center (DLR), 82234 Wessling, Germany (e-mail: c.dellasantina@tudelft.nl).

This article has supplementary material provided by the authors and color versions of one or more figures available at https://doi.org/10.1109/TMECH.2024.3402321.

Digital Object Identifier 10.1109/TMECH.2024.3402321

I. Introduction

QUADRUPEDAL robots are capable of performing in various locomotion modalities, combining the advantage of legged robotics within an inherently stable solution [1], [2], [3]. To improve robustness, increase energy efficiency, or realize highly dynamic motions, passive elastic elements can be integrated into the complex robotic system [4], [5], [6], [7], resulting in articulated soft quadrupeds (also called elastic, elastically actuated, or compliant quadrupeds) [8]. Among these, parallel elastic actuators (PEAs)-based systems have shown effectiveness in several works. For example, the authors in [7], [9], and [10] demonstrated that PEAs can provide considerable energetic benefits. Grimmer et al. [11] argued that this elastic actuation modality aids in reducing peak power. Finally, Santina and Albu-Schaeffer [12] discussed using them to generate hyperefficient oscillatory motions. These results are, however, mostly demonstrated in a simplified setting, and relatively few full-fledged PEA-driven quadrupeds have been proposed and validated so far. The pioneering PUPPY II [13] integrated parallel springs in its knee joints, as the more recent Cheetah-cub [14], Oncilla [15], and the modified ANYmal in [16]. SpaceBok [17] and Morti [18] are instead planar quadrupeds with parallel springs acting independently on all sagittal joints. Also, these designs are unique and often hard to replicate. Aside from this, the effective template model for explosive locomotion exploiting parallel compliance needs further study.

This work designs an enhanced Go (E-Go) robot (see Fig. 1), the easy-to-implement quadruped with parallel springs on all joints.[1] With this delicate design, we achieve energy-efficient locomotion. Furthermore, we realize controlled explosive motion with parallel compliance based on a novel template model. Inspired by the work in [20], we open-source the system, including the design and controller, to prompt research in compliant locomotion. The contributions are three-fold.

i) Design of lightweight, compact, and easy-to-reproduce *mechanical add-ons*, which endow Unitree's Go1 with passive compliance—yielding the E-Go robot.
ii) Developing a *control system*, including an explosive motion planner based on a novel spring-loaded inverted pendulum (SLIP) model and a hybrid torque controller.

[1]Previously used in learning algorithm validation [19], but not the focus of that work.

Fig. 1. Delft E-Go, the compliant quadruped with parallel elasticity, stores energy in springs (left) and releases it for an explosive jump (right).

iii) *Extensive experiments* demonstrating the reliability of system design, showing the energetic benefits of the PEAs, and the enhanced locomotion capability.[2] Particularly, the controlled pronking of a quadruped with asymmetric legs is first achieved with this system.

We then briefly detail contributions (i) and (ii) as follows.

A. Hardware Add-Ons

Our primary goal is to propose an accessible, compliant quadrupedal system that is easily replicated. So, rather than designing a robot from scratch, we propose a set of lightweight mechanical add-ons that turn the commercial robot, e.g., Unitree Go1 [3] into a compliant quadruped. To encourage research and experimentation, all elastic elements can be easily replaced to test the effect of different stiffnesses or to compare against the no-spring case. Section II details the design.

B. Modeling and Control

The control architecture[3] comprises two modules: a motion planner and a low-level tracking controller.

Trajectory optimization (TO) [21], [22], [23] has been used for explosive locomotion but lacks parallel compliance due to the assumption of rigid dynamics. The SLIP model, with few parameters, effectively captures compliant dynamics and adapts to tasks like pronking, hopping, and running [19], [24], [25], [26], [27]. Particularly, the dual-SLIP version provides insights into two-leg motions [28]. However, the current dual-SLIP model did not model the parallel compliance explicitly. To tackle this issue, we propose a novel 3-D actuated dual-SLIP model, which decouples actuation and parallel compliance. Based on this simplified model, a TO is formulated to generate versatile explosive motion without requiring reference motions. Section III details the dual-SLIP model and motion planner.

The torque controller is then employed to track reference precisely without defeating the purpose of PEA design. To this end, we propose to use anticipatory control—taking inspiration from what is proposed in soft manipulators [29], by combining it with optimal control for feedforward torque compensation borrowed from rigid quadrupeds literature [30]. Finally, through incorporating feedback tracking control, a hybrid control scheme is formulated, as detailed in Section IV.

[2]The video is available at: https://youtu.be/egQq9bRwqW4.

[3]This is not an extension of Unitree's software but an entirely novel controller. Unitree's architecture cannot be directly applied nor adapted to factor in the springs' effect.

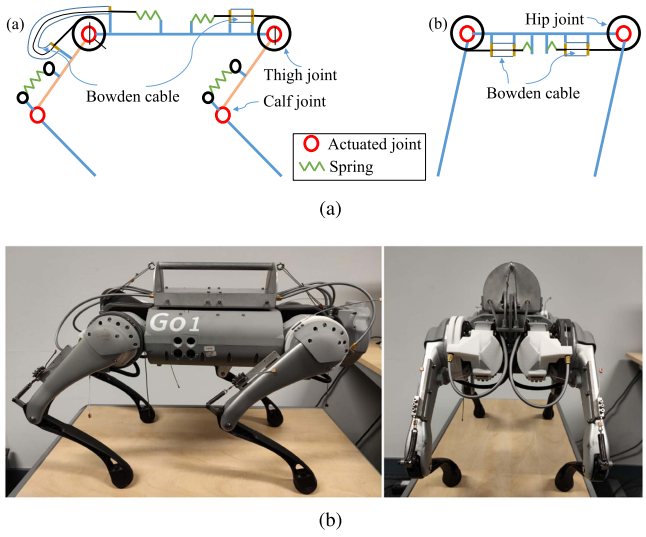

Fig. 2. Panel (a) reports a pictorial representation of the topology of interconnection of the parallel elastic springs. The left part details the cable-driven PEA design on the thigh joint and the mono-articulated PEA on the calf joint. The right part details the cable-driven PEA design on the hip joint. Similar views of the robot are reported for comparison in panel (b). (a) Parallel springs topology. (b) Side view (left) and back view (right) of E-Go.

Notation: Matrices and vectors are separately noted by bold normal and italic fonts. For a matrix, the subscript $(\cdot)_{(i)}$ means the ith column and $(\cdot)_{(j,i)}$ notes the element at the jth row and ith column. For a vector, $(\cdot)_{(i)}$ refers to the ith element.

II. Hardware Design

This section presents the hardware design of E-Go, by highlighting the differences with existing designs.

A. Topology

To achieve energy-efficient locomotion while encouraging explosive motion, we need to store the potential energy while squatting down and then release it when stretching the leg. Therefore, we propose to use the configuration in Fig. 2(a), whereby the attached springs are tensioned when the thigh joint rotates clockwise, and the calf joint rotates anticlockwise.

As visualized in Fig. 2(a), two types of PEA configurations are employed on the quadrupedal robot, i.e., cable-driven PEA on the hip and thigh joints and mono-articulated PEA on the calf joint. In hip and thigh joints, Bowden cables are used for force and motion transmission [also see Fig. 2(b)], which is different from the existing works such as [31] and [18] where a string-driven structure is used. The introduction of Bowden cables allows for a flexible placement, alleviating the potential interference between the string motion and the link motion. Also, differing from the previous studies, such as [14] and [32], which adopt biarticulated PEA for calf joint actuation, we design a simplified mono-articulated structure. As a result, this spring deformation is merely determined by the calf rotation, reducing the modeling complexity.

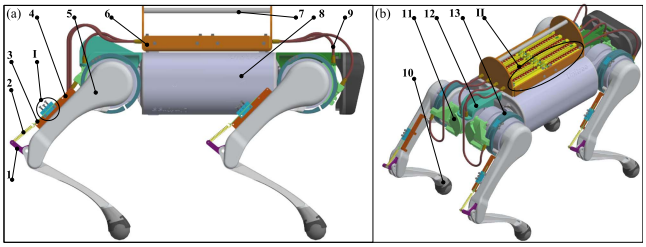

Fig. 3. 3-D model of the robot. (a) Side view. (b) 3-D rendering. Here, 1-thigh link, 2-calf spring, 3-pretensioned (rigid) string, 4-positioning board, 5-thigh link shelf, 6-guide slot base, 7-handlebar, 8-body cover, 9-Bowden cable tube, 10-force sensor, 11-connection flange between the thigh joint and a PEA, 12-connection flange between the hip joint and a PEA, 13-bracket.

Fig. 4. Installation of the spring engaging mechanism: left is for the hip joint, middle the thigh joint, and right the calf joint.

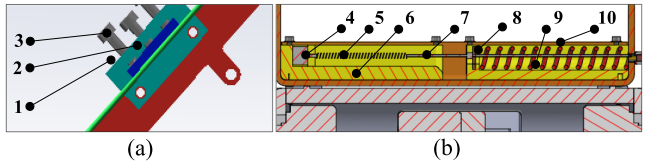

Fig. 5. Detailed views of the assemblies "I" and "II" in Fig. 3. (a) Partial view of the spring engaging mechanism (e.g., the one attached to the calf joint), and (b) sectional view of the spring pretension/guide mechanism. Here, 1-spring engaging flange, 2-compression board, 3-compression bolt, 4-connection block, 5-pretensioned soft spring, 6-guide slot, 7-Bowden cable, 8-clamp, 9-parallel tension spring, 10-sealing cover.

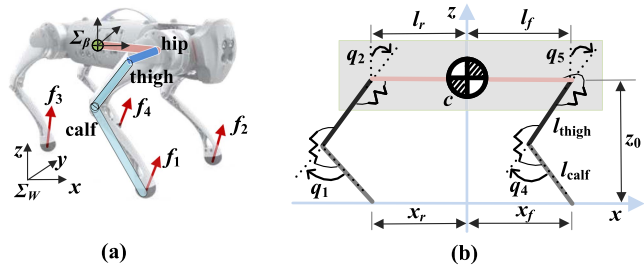

Fig. 6. E-Go joint notation (a) and its sagittal PEA arrangement (b). (b) Robot is placed at the homing pose, with $z_0 = 0.3$ m. We call q_1, q_4 the calf angles, q_2, q_5 the thigh angles, and q_3, q_6 the hip angles.

B. Design of PEA Add-Ons

Following the abovementioned topology, we design a novel compliant quadrupedal robot based on the Unitree Go1 robot, with PEAs applied in all the actuated joints, leading to the E-Go in Fig. 2(b). An overview of the 3-D model can be found in Fig. 3. Particularly, a lightweight spring engaging mechanism, described by "I" in Fig. 3(a), is used on all the joints. Besides, a compact spring pretension/guide mechanism is designed for PEAs that are attached to hip and thigh joints.

1) Spring Engaging With Adjustable Rest Length: The same spring engaging mechanism ["I" in Fig. 3(a)] is applied to all actuated joints, which is separately installed on the flange connected to the hip joint [see part 9 in Fig. 3(b)], on the bracket around the thigh joint [see part 11 in Fig. 3(b)], and on the positioning board [4 in Fig. 3(a)]. A real photo of the assembly is found in Fig. 4.

Fig. 5(a) shows that the engaging mechanism mainly consists of one spring engaging flange (part 1), one compression board (part 2), and three compression bolts (part 3), forming a lightweight and compact assembly. In practical uses, one can press the rigid pretensioned cable to the flange by tightening the compression bolts. In this way, we can control the pretensioning force and adjust the rest length, providing adaptability to different homing configurations.

2) Spring Pretension/Guide Mechanism: The spring units for the hip and thigh joints are placed on top of the body, where the guide mechanism is introduced, see "II" in Fig. 3(b). One sectional view in Fig. 5(b) reveals that the system mainly consists of a soft pretensioned cable (part 5), a parallel spring (part 9), and the Bowden cable (part 7). Taking the thigh joint as an example, one can engage the parallel spring by tightening the Bowden cable using the spring engaging mechanism installed on the bracket, i.e., part 13 in Fig. 3(b). By imposing different pretensioning forces, the rest length of the parallel spring can also be adjusted.

The total PEA add-ons weigh about 1.5 kg, which is lightweight compared with the body weight (about 12 kg). Also, since most of the PEA units are placed above the body, our design does not weaken the kinematic reachability of the original Go1 robot.

C. PEA Stiffness

Fig. 6(a) describes the E-Go joint configuration, and Fig. 6(b) illustrates the resultant PEA arrangement in the sagittal plane. In real applications, PEA parameters such as spring rest angle and spring constants can be determined according to different task requirements. Here, assuming that the rest angle matches the homing pose [see Fig. 6(b)], we derive a feasible range of spring constants.

In the sagittal plane, we consider that the robot can tension the springs when squatting down to the lowest height ($\underline{z}$), by imposing a certain joint torque. In this way, the robot stores the potential energy in the leg retraction process and releases energy when stretching its legs. The stiffest spring with maximal spring constant ($\overline{k}$) is tensioned when using the maximal torque ($\overline{\tau}$) output by the motor. For the ith actuated joint [i.e., thigh and calf joint in Fig. 6(a)], we have

$$\overline{\tau}_i^{\mathrm{s}}(\underline{z}) = \overline{k}_i \left(q_i(\underline{z}) - q_i^0\right) = \tau_i^{\mathrm{g}}(\underline{z}) + \overline{\tau}_i \tag{1}$$

TABLE I
MODELING PARAMETERS OF THE E-GO ROBOT

joint	$\overline{k}$ [N·m/rad]	q^0 [rad]	torque limit [N·m]	link length [m]
hip	23	0	23.7	0.127
thigh	42	0.72	23.7	0.213
calf	21	−1.44	31.5	0.213

where q_i^0 is the ith joint angle when the robot is in the homing pose, i.e., $z = z_0$ [see Fig. 6(b)], $q_i(\underline{z})$ is the ith joint angle when the robot reaches the lowest height, i.e., $z = \underline{z}$. $\tau_i^{\mathrm{g}}(\underline{z})$ is the ith joint torque due to the gravity effect.

In (1), we assume that the springs start to be engaged when putting the leg in the homing pose. Besides, $\underline{z}$ is set to be 0.12 m to avoid body collision with the ground. Using the maximal torque $\overline{\tau}$ in Table I, the $\overline{k}$s of the thigh and calf joint could be computed.

In addition, the hip spring is chosen such that the robot can fully swing the leg sideways using the maximal torque output. The resultant spring constants are listed in Table I.[4]

III. SLIP-BASED DYNAMIC MOTION PLANNING

In this section, we first introduce a novel 3-D actuated dual-SLIP model, which characterizes parallel compliance explicitly. Then, taking the quadrupedal pronking as an example, we detail the TO formulation for explosive motion planning.

A. 3-D Actuated Dual-SLIP With Parallel Compliance

Through pairing the four legs into two groups, we propose a dual SLIP model to model the quadrupedal dynamics by explicitly considering the parallel compliance. Decoupling the actuation and parallel elasticity, we have

$$\begin{aligned} \text{Stance:} \quad & \ddot{\boldsymbol{c}} = \frac{\boldsymbol{F}_s^1 + \boldsymbol{F}_s^2 + \boldsymbol{F}_a^1 + \boldsymbol{F}_a^2}{m} + \boldsymbol{g} \\ \text{Flight:} \quad & \ddot{\boldsymbol{c}} = \boldsymbol{g} \end{aligned} \tag{2}$$

where $\boldsymbol{F}_a^1 \in \mathbb{R}^3$ and $\boldsymbol{F}_a^2 \in \mathbb{R}^3$ are the actuation force on leg 1 and leg 2, respectively. $\boldsymbol{F}_s^1 \in \mathbb{R}^3$ and $\boldsymbol{F}_s^2 \in \mathbb{R}^3$ are the elastic forces on leg 1 and leg 2, respectively, $\ddot{\boldsymbol{c}} \in \mathbb{R}^3$ is the center of mass (CoM) acceleration, $\boldsymbol{g} \in \mathbb{R}^3$ is the gravitational acceleration, $m \in \mathbb{R}$ is the total mass.

In (2), $\boldsymbol{F}_s^1$ and $\boldsymbol{F}_s^2$ are computed by

$$\boldsymbol{F}_s^1 = k_s^1(l_0^1 - ||\boldsymbol{l}_1||_2)\hat{\boldsymbol{l}}_1, \quad \boldsymbol{F}_s^2 = k_s^2(l_0^2 - ||\boldsymbol{l}_2||_2)\hat{\boldsymbol{l}}_2 \tag{3}$$

where $k_s^1 \in \mathbb{R}$ and $k_s^2 \in \mathbb{R}$ separately denote the equivalent spring constant on leg 1 and leg 2, $\boldsymbol{l}_1 = \boldsymbol{c} - \boldsymbol{p}_r \in \mathbb{R}^3$ and $\boldsymbol{l}_2 = \boldsymbol{c} - \boldsymbol{p}_f \in \mathbb{R}^3$ are the leg vectors, with $\boldsymbol{p}_r \in \mathbb{R}^3$ and $\boldsymbol{p}_f \in \mathbb{R}^3$ being the leg positions. $\hat{\boldsymbol{l}}_1 \in \mathbb{R}^3$ and $\hat{\boldsymbol{l}}_2 \in \mathbb{R}^3$ are the unit leg vectors. $l_0^1 \in \mathbb{R}$ and $l_0^2 \in \mathbb{R}$ are the rest lengths. $||\cdot||_2$ here obtains the L_2 norm of a vector.

Note that, in this dual-SLIP model, k_s^1 and k_s^2 are the equivalent spring constants of the parallel springs.[5] That is, k_s^1 and k_s^2 are zeros when no spring is engaged, which is not achieved by the traditional dual-SLIP model [28].

Remark 1: The decoupling of the actuation and the parallel compliance enables the SLIP model to be applied to both rigid (without parallel springs) and compliant (with parallel springs) cases. Furthermore, the spring constants of two legs can vary from each other, meaning that the dual-SLIP model can be applied to quadrupeds with asymmetric legs, which, however, is impossible using the single-leg model [19], [24], [25], [26].

B. Pronking Motion Optimization

Based on the actuated dual-SLIP model, we generate pronking motions, with all feet lifting off and touching down simultaneously. Assuming N_s knots for the stance phase (each knot lasts t_s) and N_f knots for the flight phase (each knot lasts t_f), we define a TO as

$$\arg \min_{\mathbf{X},\mathbf{F}_a^1,\mathbf{F}_a^2,\mathbf{q},\boldsymbol{t}} \quad J_{\text{cost}} \tag{4a}$$

$$\text{s.t.} \quad \mathbf{X}_{(1)} = \boldsymbol{X}_0, \quad \dot{\mathbf{X}}_{(1)} = \dot{\boldsymbol{X}}_0, \quad \mathbf{q}_{(1)} = \boldsymbol{q}_0 \tag{4b}$$

$$(1-\xi)z_t \le \boldsymbol{X}_{z(N_s)} \le (1+\xi)z_t \tag{4c}$$

$$(1-\xi)\lambda^r \le \boldsymbol{X}_{\lambda(N_s+N_f)} \le (1+\xi)\lambda^r, \lambda \in \{x, y\} \tag{4d}$$

$$\boldsymbol{X}_{z(N_s+N_f)} = z^r \tag{4e}$$

$$\underline{\boldsymbol{t}} \le \boldsymbol{t} \le \overline{\boldsymbol{t}} \tag{4f}$$

$$\forall k \in [1, 2, \ldots, N_s + N_f - 1]$$

$$\mathbf{X}_{(k+1)} = \mathbf{X}_{(k)} + \dot{\mathbf{X}}_{(k)}t + 0.5\ddot{\mathbf{X}}_{(k)}t^2 \tag{4g}$$

$$\dot{\mathbf{X}}_{(k+1)} = \dot{\mathbf{X}}_{(k)} + \ddot{\mathbf{X}}_{(k)}t \tag{4h}$$

$$\forall k \in [1, 2, \ldots, N_s]$$

$$\ddot{\mathbf{X}}_{(k)} = \frac{\mathbf{F}_s^1(\mathbf{X}_{(k)}) + \mathbf{F}_s^2(\mathbf{X}_{(k)}) + \mathbf{F}_{a(k)}^1 + \mathbf{F}_{a(k)}^2}{m} + \boldsymbol{g} \tag{4i}$$

$$0 \le \boldsymbol{F}_{z(k)}^i + \boldsymbol{F}_{s,z}^i(\mathbf{X}_{(k)}) \le \overline{F}_z, i \in \{1, 2\} \tag{4j}$$

$$-\mu \le \ddot{\boldsymbol{X}}_{\lambda(k)}/(\ddot{\boldsymbol{X}}_{z(k)} + g) \le \mu, \lambda \in \{x, y\} \tag{4k}$$

$$\underline{\boldsymbol{q}} \le \mathbf{q}_{(k)} \le \overline{\boldsymbol{q}} \tag{4l}$$

$$\mathrm{FK}(\mathbf{q}_{(k)}, \boldsymbol{p}) = \mathbf{X}_{(k)} \in \mathrm{conv}[\boldsymbol{p}] \tag{4m}$$

$$\forall k \in [N_s + 1, \ldots, N_s + N_f - 1]$$

$$\ddot{\boldsymbol{X}}_{(k)} = \boldsymbol{g} \tag{4n}$$

where decision variables contain $\mathbf{X}$, $\mathbf{F}_a^1$, $\mathbf{F}_a^2$, $\mathbf{q}$, and $\boldsymbol{t}$. $\mathbf{X} \in \mathbb{R}^{3\times(N_s+N_f)}$ comprises the sagittal ($\boldsymbol{X}_x \in \mathbb{R}^{N_s+N_f}$), lateral ($\boldsymbol{X}_y \in \mathbb{R}^{N_s+N_f}$), and vertical ($\boldsymbol{X}_z \in \mathbb{R}^{N_s+N_f}$) CoM positions, $\mathbf{F}_a^1 \in \mathbb{R}^{3\times N_s}$ consists of the sagittal ($\boldsymbol{F}_x^1 \in \mathbb{R}^{N_s}$), lateral ($\boldsymbol{F}_y^1 \in \mathbb{R}^{N_s}$), and vertical ($\boldsymbol{F}_z^1 \in \mathbb{R}^{N_s}$) actuation force on leg 1 during the stance phase, $\mathbf{F}_a^2 \in \mathbb{R}^{3\times N_s}$ denotes the actuation force on leg 2, $\mathbf{F}_s^1 \in \mathbb{R}^{3\times N_s}$ consists of the sagittal ($\boldsymbol{F}_{s,x}^1 \in \mathbb{R}^{N_s}$), lateral ($\boldsymbol{F}_{s,y}^1 \in \mathbb{R}^{N_s}$), and vertical ($\boldsymbol{F}_{s,z}^1 \in \mathbb{R}^{N_s}$) elastic force on leg 1, $\mathbf{F}_s^2 \in \mathbb{R}^{3\times N_s}$ denotes the elastic force on leg 2, $\mathbf{q} \in \mathbb{R}^{12\times N_s}$ consists of joint angles during the stance phase, $\boldsymbol{t} = [t_s, t_f]^{\mathrm{T}} \in \mathbb{R}^2$ contains the step sizes for stance and flight phases, $\xi \in \mathbb{R}$ is the slack variable.

[4]Other objects can be used when choosing PEA parameters. For example, one can expect the robot to support itself with parallel springs without extra motor torque inputs. We left the parameter optimization as a future work.

[5]They can be derived following the Lagrange mechanics. Details are omitted here.

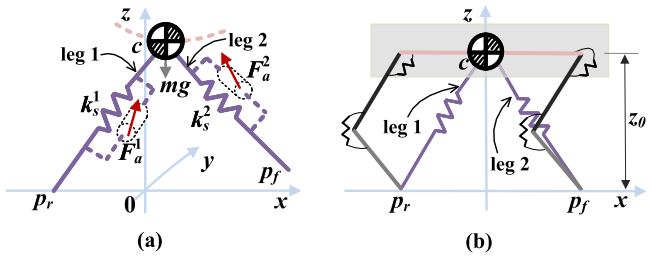

Fig. 7. (a) 3-D actuated dual-SLIP model with parallel compliance and (b) sagittal motion mapping in the homing pose.

1) Cost Function: The cost function in (4a) is defined as

$$J_{\text{cost}} = J_{\text{stance}} + J_{\text{flight}} + J_{\text{land}} + J_t + J_q \tag{5a}$$

with

$$J_{\text{stance}} = \sum_{k=1}^{N_s} (w_F^1 \|\mathbf{F}_{a(k)}^1\|^2 + w_F^2 \|\mathbf{F}_{a(k)}^2\|^2 + w_a \|\ddot{\mathbf{X}}_{(k)}\|^2) \tag{5b}$$

$$J_{\text{flight}} = \sum_{k=N_s+1}^{N_s+N_f} w_f \|\boldsymbol{X}_{z(k)} - z_t\|^2 \tag{5c}$$

$$J_{\text{land}} = w_x \|\boldsymbol{X}_{x(Ns+Nf)} - x^r\|^2 + w_y \|\boldsymbol{X}_{y(Ns+Nf)} - y^r\|^2 \tag{5d}$$

$$J_t = w_t \|\boldsymbol{t} - \boldsymbol{t}^r\|^2 \tag{5e}$$

$$J_q = \sum_{k=1}^{N_s} w_q \|\mathbf{q}_{(k)} - \boldsymbol{q}_0\|^2 \tag{5f}$$

where J_{stance} penalizes control inputs and the CoM acceleration, J_{flight} penalizes deviations from the reference shooting height z_t during the flight phase, J_{land} minimizes the tracking error of the landing position, J_t penalizes the deviation from the reference time steps ($\boldsymbol{t}^r = [t_s^r, t_f^r]^{\mathrm{T}} \in \mathbb{R}^2$), J_q penalizes the deviation from the homing angles ($\boldsymbol{q}^0 \in \mathbb{R}^{12}$), $w_F^1, w_F^2, w_a, w_f, w_x, w_y, w_t$, and w_q are the positive weights.

2) Feasbility Constraints: Equation (4b) defines the initial jumping states according to the task requirements. When starting from the homing pose with zero velocity [see Fig. 7(b)], we have

$$\boldsymbol{X}_0 = \begin{bmatrix} 0, 0, z_0 \end{bmatrix}^{\mathrm{T}}, \quad \dot{\boldsymbol{X}}_0 = \begin{bmatrix} 0, 0, 0 \end{bmatrix}^{\mathrm{T}}. \tag{6}$$

Meanwhile, $\boldsymbol{q}_0$ is calculated by the inverse kinematics. Equation (4c) limits the shooting height at the take-off moment. In order to jump longer and higher, the robot should shoot at a big height with a large shooting velocity. To this end, we guess the nominal shooting height as

$$z_t = \sqrt{(l_{\text{thigh}} + l_{\text{calf}})^2 - l_f^2} \tag{7}$$

where $l_{\text{thigh}}, l_{\text{calf}}, l_f$ separately denote the thigh link length, calf link length, and front thigh offset, as depicted in Fig. 6(b).

Equations (4d)–(4e) define the landing states when touchdown, with $[x^r, y^r, z^r]^{\mathrm{T}}$ being the target landing position. Note that, to enhance the solvability, we use soft constraints in (4c)–(4d), with ξ being a small value.

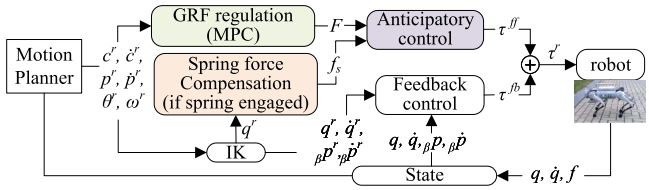

Fig. 8. Overall control flow of the E-Go quadrupedal robot.

Equation (4f) limits the time duration of each step, with $\underline{\boldsymbol{t}} \in \mathbb{R}^2$ and $\overline{\boldsymbol{t}} \in \mathbb{R}^2$ being the lower and upper boundaries.

Equations (4g)–(4h) describes the state transition between neighboring knots. In this work, we adopt the Euler integration to guarantee the continuity, using the respective step size t, i.e., t_s ($\boldsymbol{t}_{(1)}$) for the stance phase and t_f ($\boldsymbol{t}_{(2)}$) for the flight phase, and the corresponding acceleration [computed using (4i) during the stance phase and by (4n) during the flight phase].

Equations (4j) guarantees that the generated ground reaction force is within a feasible range, where $\overline{F}_z$ is the maximal vertical force. Furthermore, (4k) prevents slippage during the stance phase, with μ being the friction coefficient.

Equation (4l) constrains the joint motion, with $\underline{\boldsymbol{q}} \in \mathbb{R}^{12}$ and $\overline{\boldsymbol{q}} \in \mathbb{R}^{12}$ being the lower and upper boundaries.

Equation (4m) restricts the CoM position within the kinematics reachability, with $\boldsymbol{p} \in \mathbb{R}^{12}$ being support positions. $\mathrm{FK}(\cdot)$ is the forward kinematics operatior.

Using the abovementioned TO formulation, we can achieve the optimal pronking motion. Note that this planner can be applied to rigid and compliant cases, which would be validated in Section V-D.

Remark 2: Using the proposed TO formulation, the full-body kinematics are considered when generating a dynamic motion, similar to the kino-dynamic framework in [33]. However, since the SLIP model is incorporated in our formulation, reference joint trajectories for the jumping motion are not required, unlike the kino-dynamic optimization in [23] and [34].

IV. Locomotion Control Scheme

This section presents the hybrid control strategy, i.e., anticipatory control (feedforward control, generating τ^{ff}) plus feedback control (generating τ^{fb}) for motion tracking. As illustrated in Fig. 8, we employ the model predictive control (MPC) to optimize the desired ground reaction force (GRF) on each stance foot. When parallel springs are engaged, the spring torque compensation is activated.

A. GRF Compensation

To be simple, we model the quadrupedal robot as a single rigid body (SRB) with four mass-less legs [30], resulting in

$$\ddot{\boldsymbol{c}} = \frac{\sum_{j=1}^{4} \boldsymbol{f}_j}{m} + \boldsymbol{g}, \quad \mathbf{I}\dot{\boldsymbol{\omega}} \cong \sum_{j=1}^{4} (\boldsymbol{p}_j - \boldsymbol{c}) \times \boldsymbol{f}_j \tag{8}$$

where $\boldsymbol{f}_j \in \mathbb{R}^3$ and $\boldsymbol{p}_j \in \mathbb{R}^3$ separately denote the GRF and position on the jth leg ($j \in \{1, \ldots, 4\}$), $\dot{\boldsymbol{\omega}} \in \mathbb{R}^3$ is the angular

acceleration, $\mathbf{I} \in \mathbb{R}^{3\times3}$ is the inertia tensor in the world frame, $\times$ denotes the cross-product operation.

To compute the optimal GRF, we introduce an MPC scheme, followed by

$$\arg\min_{\mathbf{F},\ddot{\mathbf{S}}} \sum_{k=1}^{N_h} \|\mathbf{S}_{(k)} - \mathbf{S}^r_{(k)}\|^2_{\mathbf{Q}} + \|\ddot{\mathbf{S}}_{(k)}\|^2_{\mathbf{R}} + \|\mathbf{F}_{(k)}\|^2_{\mathbf{L}} \tag{9a}$$

$$\text{s.t.} \quad \text{State transition:} \quad \mathbf{S}_{(k)} = \mathbf{A}\mathbf{S}_{(k-1)} + \mathbf{B}\ddot{\mathbf{S}}_{(k)} \tag{9b}$$

$$\text{Dynamics constraints:} \quad \ddot{\mathbf{S}}_{(k)} = \text{SRB}(\mathbf{c}_{(k)}, \mathbf{F}_{(k)}) \tag{9c}$$

$$\text{Contact condition:} \quad \mathbf{D}^j_{(k)}\mathbf{F}^j_{(k)} = \mathbf{0} \tag{9d}$$

$$\text{GRF constraints:} \quad \mathbf{F}^j_{(k)} \in \mathbb{S} \tag{9e}$$

where N_h denotes the length of the prediction horizon, system state $\mathbf{S} \in \mathbb{R}^{12\times N_h}$ consists of 3-D CoM position, body angles, CoM velocity and angular velocity, control inputs include the 3-D linear and angular accelerations, i.e., $\ddot{\mathbf{S}} \in \mathbb{R}^{6\times N_h}$ and GRFs on all legs, i.e., $\mathbf{F} \in \mathbb{R}^{12\times N_h}$. Specifically, $\mathbf{F}^j \in \mathbb{R}^{3\times N_h}(j \in \{1,\ldots,4\})$ is the GRF on the jth leg.

1) Objective Function: The objective function in (9a) penalizes the tracking errors with minimal control efforts. The reference motion $\mathbf{S}^r$ is generated in advance. $\mathbf{Q} \in \mathbb{R}^{12\times12}$, $\mathbf{R} \in \mathbb{R}^{6\times6}$, and $\mathbf{L} \in \mathbb{R}^{12\times12}$ are the diagonal weight matrices.

2) Feasibility Constraints: The state transition is processed in (9b), where $\mathbf{A}$ and $\mathbf{B}$ are computed offline following the Taylor expansion (see [35]). Note that the real state is chosen as the initial state (i.e., $\mathbf{S}_{(0)}$) in (9b). The SRB dynamics are obeyed using (9c), where

$$\text{SRB}(\mathbf{c}_{(k)}, \mathbf{F}_{(k)}) = \begin{bmatrix} \mathbf{I}_{3\times3} & \cdots & \mathbf{I}_{3\times3} \\ [\mathbf{p}^1_{(k)} - \mathbf{c}^r_{(k)}]_\times & \cdots & [\mathbf{p}^4_{(k)} - \mathbf{c}^r_{(k)}]_\times \end{bmatrix} \mathbf{F}_{(k)} + \begin{bmatrix} \boldsymbol{g} \\ \mathbf{0}_{3\times1} \end{bmatrix} \tag{10}$$

where $\mathbf{p}^j_{(k)} \in \mathbb{R}^3(j \in \{1,\ldots,4\})$ denotes the jth leg position at the kth step within the prediction window, $\mathbf{c}^r_{(k)} \in \mathbb{R}^3$ denotes the reference CoM position at the kth step.

The contact complementary condition in (9d) guarantees that GRFs are only assigned to the feet that are in contact with the ground, where $\mathbf{F}^j_{(k)} \in \mathbb{R}^3$ is the 3-D GRF on the jth foot at the kth step, and $\mathbf{D}^j_{(k)} \in \mathbb{R}$ is the nonnegative distance between the ground and the jth foot at the kth step. Equation (9e) guarantees the feasible GRFs by obeying the unilateral contact constraints and friction cone constraints. Details are omitted here.

The abovementioned MPC could be solved efficiently by off-the-shelf QP solvers. Then, feedforward torque compensating for the desired GRF of the jth leg is calculated by

$$\boldsymbol{\tau}^{\text{GRF}}_j = -\mathbf{J}^{\text{T}}_j \mathbf{F}^j_{(1)} \tag{11}$$

where $\mathbf{J}_j \in \mathbb{R}^{3\times3}$ and $\boldsymbol{\tau}^{\text{GRF}} \in \mathbb{R}^3$ separately denote the contact Jacobian and torque command.

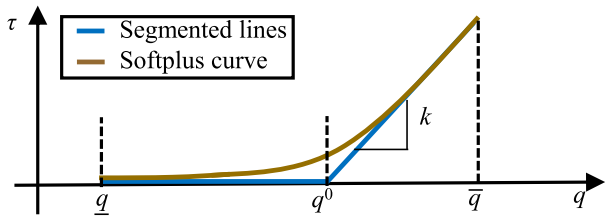

Fig. 9. Nonlinear torque profile of parallel springs. $\underline{q}$ and $\bar{q}$ separately denote the minimal and maximal allowable joint angles.

B. Compliance Compensation

The SRB dynamics used in the abovementioned MPC do not account for the parallel compliance introduced by the PEA add-ons. To tackle this issue, we compensate for the spring torques using another anticipatory controller. In E-Go, only unilateral force is generated by the spring unit when it is tensioned. Taking the thigh joint, for example, the spring torque τ^s is

$$\tau^s = \begin{cases} 0, & q^r \le q^0 \\ k(q^r - q^0), & q^r > q^0 \end{cases} \tag{12}$$

where q^r and q^0 separately denote the desired angle and the rest length of the thigh joint, k is the spring constant. To avoid abrupt variations in the spring torque, we use a softplus function to approximate the segmented lines determined by (12). As illustrated in Fig. 9, the spring torques for the jth leg are

$$\boldsymbol{\tau}^s_j = \ln(1 + \exp(\mathbf{K}_j(\boldsymbol{q}^r_j - \boldsymbol{q}^0_j))) \tag{13}$$

where $\ln(\cdot)$ and $\exp(\cdot)$ separately denote the natural logarithm and exponential functions, $\boldsymbol{\tau}^s_j \in \mathbb{R}^3$ and $\boldsymbol{q}^r_j \in \mathbb{R}^3$ are the spring torques and reference joint angles of each leg. $\mathbf{K}_j \in \mathbb{R}^{3\times3}$ is a diagonal matrix, taking the spring constants on three joints of the jth leg as the diagonal values.

C. Leg Motion Control

We control the stance leg and swing leg, as follows.

1) Stance Leg: GRF generated by MPC is imposed on the stance leg to drive the body motion. Taking the jth leg, for example, the commanded joint torque ($\boldsymbol{\tau}^j_{\text{stance}} \in \mathbb{R}^3$) is then computed by considering feedback ($\boldsymbol{\tau}^{\text{fb}}_{\text{stance}} \in \mathbb{R}^3$) and feedforward terms ($\boldsymbol{\tau}^{\text{ff}}_{\text{stance}} \in \mathbb{R}^3$), as follows:

$$\boldsymbol{\tau}^j_{\text{stance}} = \boldsymbol{\tau}^{\text{ff}}_{\text{stance}} + \boldsymbol{\tau}^{\text{fb}}_{\text{stance}} \tag{14}$$

where the feedforward term $\boldsymbol{\tau}^{\text{ff}}_{\text{stance}}$ consists of the GRF compensation [in (11)] and the spring compensation [in (13)], the feedback term $\boldsymbol{\tau}^{\text{fb}}_{\text{stance}}$ is obtained by the joint-space impedance control (see [30]).

2) Swing Leg: After lifting off from the ground, the swing leg follows the desired trajectory. To this end, the spring torque feedforward compensation and the impedance feedback control are incorporated. For the jth leg, we have

$$\boldsymbol{\tau}^j_{\text{swing}} = \boldsymbol{\tau}^{\text{ff}}_{\text{swing}} + \boldsymbol{\tau}^{\text{fb}}_{\text{swing}} \tag{15}$$

where the feedforward term $\boldsymbol{\tau}^{\text{ff}}_{\text{swing}}$ compensates for Coriolis, gravity, and spring deformation, the feedback term $\boldsymbol{\tau}^{\text{fb}}_{\text{swing}}$ is

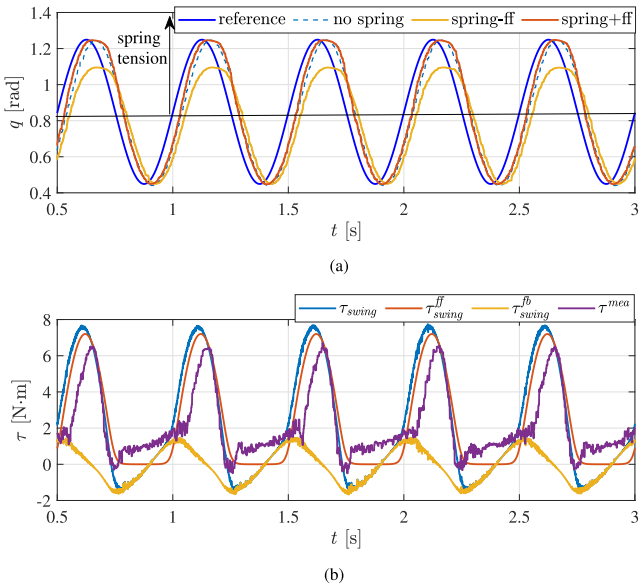

Fig. 10. Angle and torque profiles of the thigh joint. (a) "No spring," "spring-ff," and "spring+ff" separately represent the joint rotation without the spring engaged, the joint rotation with the spring engaged but no feedforward spring torque compensation, and the spring engagement with compensation. (b) Plots the torque profiles in the "spring+ff" mode.

obtained by the joint-space impedance control and leg movement tracking control (see [30]).

V. Evaluations

This section validates the performance of E-Go with parallel compliance. We start by evaluating motion tracking performance using the hybrid control strategy. Then, we analyze the energy benefits of the PEA design. Afterwards, we demonstrate locomotion capability via hardware experiments.

A. Motion Tracking With Parallel Compliance

1) Joint Tracking: Take the thigh joint on the rear right (RR) leg as an example, we first analyze joint behaviors when the E-Go is hung in the air. The joint angle profiles in different modes are reported in Fig. 10(a). Besides, the torque profiles when enabling the feedforward spring torque compensation (i.e., the "spring+ff" mode) are reported in Fig. 10(b).

In all three cases, namely, "no spring," "spring-ff," and "spring+ff," we commanded the robot to track the same sinusoidal curve. When the thigh angle goes above 0.83 rad, the spring is tensioned (the spring constant in the thigh joint is 16 N·m/rad). As can be seen from Fig. 10(a), the anticipatory spring force compensation, i.e., $\boldsymbol{\tau}^s_j$ in (13), contributes to a decent tracking performance (see the red curve). In contrast, without spring compensation, the reference angle cannot be tracked when the spring is tensioned, see the yellow curve in Fig. 10(a). From Fig. 10(b), we can find that anticipatory compliance compensation plays a crucial role in generating the desired torque when the spring is tensioned.

2) Motion Tracking With Height Variation: To further validate the tracking performance, we put the E-Go on the ground and commanded it to track a periodic height. In this case, the spring with $k = 7$ N·m/rad is also installed in the calf joint.

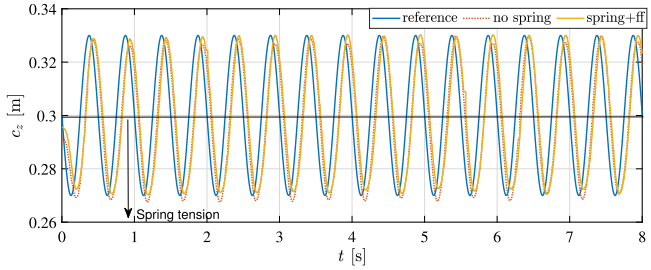

Fig. 11. Height tracking profiles. The black arrow means that the spring is tensioned when the body is below 0.3 m.

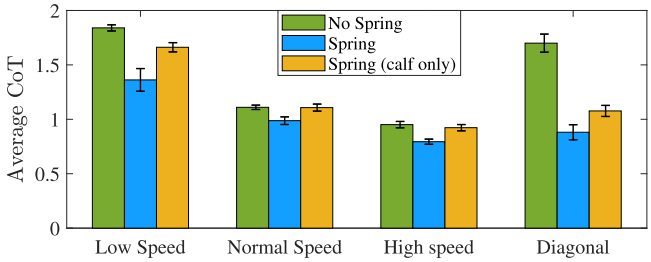

Fig. 12. CoT w.r.t. trotting speed. "No spring," "spring," and "spring (calf)" separately denote the rigid robot without springs, the compliant robot with springs fully engaged and the compliant robot with springs in the calf joints.

In Fig. 11, when the spring was not engaged (the "no spring" case), only the MPC works in the feedforward channel. It turns out that decent tracking performance could be achieved in this case. When the spring is engaged with the forward compliance compensation (the "spring+ff" case), it also achieves a good tracking performance. Compared with "no spring" case, the peak height and the lowest height were both increased, meaning that the parallel springs enhanced the joint.

B. Energetic Performance of PEA Design

With the hybrid torque controller, E-Go walks[6] on flat ground with different velocities, including at 0.1 m/s ("low speed") forward walking, 0.17 m/s ("normal speed") forward walking, 0.25 m/s ("high speed") forward walking, and 0.17 m/s forward plus 0.1 m/s lateral ("diagonal") walking. To further analyze the energetic performance with respect to (w.r.t.) the parallel compliance, we record the data with the rigid robot ("no spring"), the compliant robot with springs fully engaged ("spring") and the compliant robot with calf springs engaged ["spring (calf only)"]. In each scenario, three trials are conducted. The average cost of transport (CoT) [37], together with standard error, is plotted in Fig. 12. As can be seen in Fig. 12, the smaller CoT is achieved with "spring (calf only)," no matter in which speed mode. Furthermore, with springs fully engaged, CoT is further

[6]The trotting gait is generated using a bipedal locomotion planner [36]. Through grouping the FL and RR legs as the left leg and the FR and RL legs as the right leg, quadruped trotting is transformed into bipedal walking.

Fig. 13. E-Go walks across a collection of uneven terrains. None of these obstacles is known to the controller. The complete videos are available as a multimedia attachment.

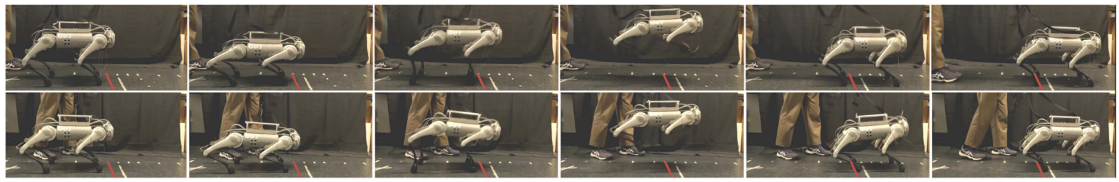

Fig. 14. 50 cm forward pronking. The first row describes the rigid pronking without springs engaged. The second row describes the compliant pronking with springs engaged.

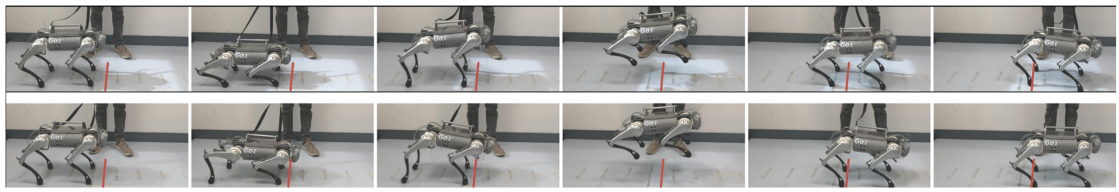

Fig. 15. 50 cm forward pronking of a quadruped with asymmetric legs. The first row describes pronking with single-leg SLIP. The second row describes the pronking with the dual-SLIP model.

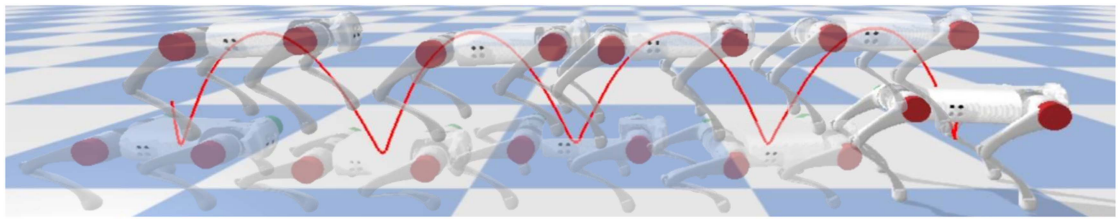

Fig. 16. Continuous pronking in PyBullet environment. The robot jumps 70 cm forward at each cycle. The red curve plots the real CoM.

reduced (in the "spring" case), demonstrating that the exploitation of parallel compliance could improve energy efficiency in quadrupedal locomotion.

C. Robust Trotting With Parallel Compliance

Robust quadrupedal locomotion across uneven terrains is tested here, where the smooth wood, antislip rubbers, and soft sponges are randomly distributed. In order to demonstrate the robustness, the robot steps with variable step parameters. It turns out that, using the proposed controller, E-Go with springs fully engaged managed to maintain balance when encountering unknown terrains. Snapshots are found in Fig. 13.

D. Explosive Pronking With Parallel Springs

Using the motion planner in Section III, pronking motions for the quadrupedal robot can be generated. With the control scheme in Section IV, pronking tasks are accomplished.

1) Enhanced Pronking: 50 cm forward pronking is displayed in Fig. 14. As can be seen from the first row, especially in the fifth picture, the rigid robot lands behind the desired landing position (marked by the red line). In contrast, when the springs are engaged, the compliant E-Go reaches the desired position. That is, the E-Go could make use of parallel compliance to enhance explosive motion.

2) Controlled Pronking With Asymmetric Legs: Using the proposed dual-SLIP model, the pronking task for the quadruped with asymmetric legs[7] could be addressed. In this scenario, we only engaged the parallel springs in the front legs. Fig. 15 (see the bottom) demonstrates that the robot could land at the desired position with a well-controlled pose. On the contrary, using the single-leg SLIP model [19], the modeling mismatch resulted in an earlier landing with large yaw errors, see the top row of Fig. 15. Note that the stance legs could move in the stance phase

[7]This kind of asymmetry can be used to model the animals with different legs or quadrupedal robotic systems with manufacturing defects.

due to the low friction of the surface. Nevertheless, our controller is robust enough to accomplish the pronking task.

Aside from this, 3-D tasks, such as diagonal pronking, are also accomplished. Please check the attached video.

3) Continuous Pronking: In the abovementioned tests, the robot starts pronking from the static homing pose, using the initial conditions defined in (6). However, the TO formulation in Section III-B could also generate versatile pronking motions with different initial conditions. Fig. 16 demonstrates the continuous four pronking with varying initial positions and velocities for each cycle. Again, it validates the effectiveness of the proposed control method.[8]

VI. Conclusion

This work proposed Delft E-Go, a quadrupedal system with parallel elasticity on each joint. We complete this mechanical design with a novel dual-SLIP model, TO-based motion planner, and a hybrid motion controller that can deal with the different dynamics generated by the proposed mechanics.[9] Hardware experiments have systematically validated the system's performance. Particularly, we highlight the energetic benefits and the explosive locomotion capability.

In this work, the spring parameters, such as the spring constant and rest length, are not optimized. In the future, we would like to optimize them by multiobjective optimization to improve the locomotion performance further.

References

[1] G. Bledt, M. J. Powell, B. Katz, J. Di Carlo, P. M. Wensing, and S. Kim, "MIT cheetah 3: Design and control of a robust, dynamic quadruped robot," in *Proc. IEEE/RSJ Int. Conf. Intell. Robot. Syst.*, 2018, pp. 2245–2252.

[2] B. Katz, J. Di Carlo, and S. Kim, "Mini cheetah: A platform for pushing the limits of dynamic quadruped control," in *Proc. IEEE Int. Conf. Robot. Autom. IEEE*, 2019, pp. 6295–6301.

[3] U. Robotics, "Unitree robot go1," 2021. [Online]. Available: https://m.unitree.com/products/go1

[4] S.-H. Chae, S.-M. Baek, J. Lee, and K.-J. Cho, "Agile and energy-efficient jumping–crawling robot through rapid transition of locomotion and enhanced jumping height adjustment," *IEEE/ASME Trans. Mechatron.*, vol. 27, no. 6, pp. 5890–5901, Dec. 2022.

[5] D. Seidel, M. Hermann, T. Gumpert, F. C. Loeffl, and A. Albu-Schäffer, "Using elastically actuated legged robots in rough terrain: Experiments with DLR quadruped bert," in *Prof. IEEE Aerosp. Conf. Proc.*, 2020, pp. 1–8.

[6] M. Hutter et al., "Anymal—A highly mobile and dynamic quadrupedal robot," in *Proc. IEEE/RSJ Int. Conf. Intell. Robot. Syst.*, 2016, pp. 38–44.

[7] W. Roozing, Z. Ren, and N. G. Tsagarakis, "An efficient leg with series–parallel and biarticular compliant actuation: Design optimization, modeling, and control of the eLeg," *Int. J. Robot. Res.*, vol. 40, no. 1, pp. 37–54, 2021.

[8] C. Della Santina, M. G. Catalano, A. Bicchi, M. Ang, O. Khatib, and B. Siciliano, "Soft robots," *Ency. Robot.*, vol. 489, pp. 1–15, 2021.

[9] M. A. Sharbafi, M. J. Yazdanpanah, M. N. Ahmadabadi, and A. Seyfarth, "Parallel compliance design for increasing robustness and efficiency in legged locomotion–theoretical background and applications," *IEEE/ASME Trans. Mechatron.*, vol. 26, no. 1, pp. 335–346, Feb. 2021.

[10] U. Mettin, P. X. La Hera, L. B. Freidovich, and A. S. Shiriaev, "Parallel elastic actuators as a control tool for preplanned trajectories of underactuated mechanical systems," *Int. J. Robot. Res.*, vol. 29, no. 9, pp. 1186–1198, 2010.

[11] M. Grimmer, M. Eslamy, S. Gliech, and A. Seyfarth, "A comparison of parallel-and series elastic elements in an actuator for mimicking human ankle joint in walking and running," in *Proc. IEEE Int. Conf. Robot. Autom.*, 2012, pp. 2463–2470.

[12] C. D. Santina and A. Albu-Schaeffer, "Exciting efficient oscillations in nonlinear mechanical systems through eigenmanifold stabilization," *IEEE Control Syst. Lett.*, vol. 5, no. 6, pp. 1916–1921, Dec. 2021.

[13] J. Buchli, F. Iida, and A. J. Ijspeert, "Finding resonance: Adaptive frequency oscillators for dynamic legged locomotion," in *Proc. IEEE/RSJ Int. Conf. Intell. Robot. Syst.*, 2006, pp. 3903–3909.

[14] A. Spröwitz, A. Tuleu, M. Vespignani, M. Ajallooeian, E. Badri, and A. J. Ijspeert, "Towards dynamic trot gait locomotion: Design, control, and experiments with cheetah-cub, a compliant quadruped robot," *Int. J. Robot. Res.*, vol. 32, no. 8, pp. 932–950, 2013.

[15] A. T. Spröwitz et al., "Oncilla robot: A versatile open-source quadruped research robot with compliant pantograph legs," *Front. Robot. AI*, vol. 5, p. 67, 2018.

[16] F. Bjelonic et al., "Learning-based design and control for quadrupedal robots with parallel-elastic actuators," *IEEE Robot. Autom. Lett.*, vol. 8, no. 3, pp. 1611–1618, Mar. 2023.

[17] P. Arm et al., "Spacebok: A dynamic legged robot for space exploration," in *Proc. IEEE Int. Conf. Robot. Autom.*, 2019, pp. 6288–6294.

[18] F. Ruppert and A. Badri-Spröwitz, "Learning plastic matching of robot dynamics in closed-loop central pattern generators," *Nature Mach. Intell.*, vol. 4, no. 7, pp. 652–660, 2022.

[19] J. Ding, M. A. van Löben Sels, F. Angelini, J. Kober, and C. Della Santina, "Robust jumping with an articulated soft quadruped via trajectory optimization and iterative learning," *IEEE Robot. Autom. Lett.*, vol. 9, no. 1, pp. 255–262, Jan. 2024.

[20] P.-A. Léziart, T. Flayols, F. Grimminger, N. Mansard, and P. Souères, "Implementation of a reactive walking controller for the new open-hardware quadruped Solo-12," in *Proc. IEEE Int. Conf. Robot. Autom.*, 2021, pp. 5007–5013.

[21] A. W. Winkler, C. D. Bellicoso, M. Hutter, and J. Buchli, "Gait and trajectory optimization for legged systems through phase-based end-effector parameterization," *IEEE Robot. Autom. Lett.*, vol. 3, no. 3, pp. 1560–1567, Jul. 2018.

[22] C. Nguyen and Q. Nguyen, "Contact-timing and trajectory optimization for 3D jumping on quadruped robots," in *Proc. IEEE/RSJ Int. Conf. Intell. Robot. Syst.*, 2022, pp. 994–999.

[23] M. Chignoli, S. Morozov, and S. Kim, "Rapid and reliable quadruped motion planning with omnidirectional jumping," in *Proc. IEEE Int. Conf. Robot. Autom.*, 2022, pp. 6621–6627.

[24] H. Geyer, A. Seyfarth, and R. Blickhan, "Compliant leg behaviour explains basic dynamics of walking and running," *Proc. Roy. Soc. B*, vol. 273, no. 1603, pp. 2861–2867, 2006.

[25] X. Xiong and A. D. Ames, "Bipedal hopping: Reduced-order model embedding via optimization-based control," in *Proc. IEEE/RSJ Int. Conf. Intell. Robot. Syst.*, 2018, pp. 3821–3828.

[26] K. Green, R. L. Hatton, and J. Hurst, "Planning for the unexpected: Explicitly optimizing motions for ground uncertainty in running," in *Proc. IEEE Int. Conf. Robot. Autom.*, 2020, pp. 1445–1451.

[27] D. Calzolari, C. Della Santina, A. M. Giordano, and A. Albu-Schäffer, "Single-leg forward hopping via nonlinear modes," in *Proc. Amer. Control Conf.*, 2022, pp. 506–513.

[28] Y. Liu, P. M. Wensing, J. P. Schmiedeler, and D. E. Orin, "Terrain-blind humanoid walking based on a 3-D actuated dual-slip model," *IEEE Robot. Autom. Lett.*, vol. 1, no. 2, pp. 1073–1080, Jul. 2016.

[29] C. Della Santina et al., "Controlling soft robots: Balancing feedback and feedforward elements," *IEEE Robot. Autom. Lett.*, vol. 24, no. 3, pp. 75–83, Sep. 2017.

[30] J. Di Carlo, P. M. Wensing, B. Katz, G. Bledt, and S. Kim, "Dynamic locomotion in the mit cheetah 3 through convex model-predictive control," in *Proc. IEEE/RSJ Int. Conf. Intell. Robot. Syst.*, 2018, pp. 1–9.

[31] A. Badri-Spröwitz, A. Aghamaleki Sarvestani, M. Sitti, and M. A. Daley, "Birdbot achieves energy-efficient gait with minimal control using avian-inspired leg clutching," *Sci. Robot.*, vol. 7, no. 64, 2022, Art. no. eabg4055.

[32] R. Sato, I. Miyamoto, K. Sato, A. Ming, and M. Shimojo, "Development of robot legs inspired by bi-articular muscle-tendon complex of cats," in *Proc. IEEE/RSJ Int. Conf. Intell. Robot. Syst.*, 2015, pp. 1552–1557.

[8] Agile pronking motion is generated offline using the measured position and velocity at the beginning of each cycle (i.e., the landing position and velocity of the previous pronking). In future, by building a motion library, we would like to demonstrate continuous pronking in real E-Go.

[9] Available at https://github.com/jtdingx/Delft-E-Go-quadruped

[33] H. Dai, A. Valenzuela, and R. Tedrake, "Whole-body motion planning with centroidal dynamics and full kinematics," in *Proc. IEEE-RAS Int. Conf. Humanoid Robots*, 2014, pp. 295–302.
[34] S. H. Jeon, S. Kim, and D. Kim, "Online optimal landing control of the mit mini cheetah," in *Proc. IEEE Int. Conf. Robot. Autom.*, 2022, pp. 178–184.
[35] J. Ding, C. Zhou, S. Xin, X. Xiao, and N. G. Tsagarakis, "Nonlinear model predictive control for robust bipedal locomotion: Exploring angular momentum and com height changes," *Adv. Robot.*, vol. 35, no. 18, pp. 1079–1097, Aug. 2021.
[36] J. Ding, X. Xiao, N. G. Tsagarakis, and Y. Huang, "Robust gait synthesis combining constrained optimization and imitation learning," in *Proc. IEEE/RSJ Int. Conf. Intell. Robot. Syst.*, 2020, pp. 3473–3480.
[37] H. C. Doets, D. Vergouw, H. E. Veeger, and H. Houdijk, "Metabolic cost and mechanical work for the step-to-step transition in walking after successful total ankle arthroplasty," *Hum. Mov. Sci.*, vol. 28, no. 6, pp. 786–797, Dec. 2009.

Jiatao Ding (Member, IEEE) received the B.Eng. and Ph.D. degrees in engineering from Wuhan University, Wuhan, China, in 2014 and 2020, respectively.

From 2018 to 2020, he was a visiting Ph.D. student with the Italian Institute of Technology, Genoa, Italy. From 2020 to 2022, he was an Assistant Research Scientist with the Shenzhen Institute of Artificial Intelligence and Robotics for Society, Shenzhen, China. He is currently a Postdoctoral Researcher with the Department of Cognitive Robotics, Delft University of Technology, Delft, The Netherlands. His research interests include optimal control and robot learning on legged locomotion.

Perry Posthoorn received the M.Sc. degree in mechanical engineering from the Delft University of Technology, Delft, The Netherlands, in 2017.

He is currently a Mechanical Engineer and Project Manager with the Electronic and Mechanical Support Division, Delft University of Technology (DEMO) and specializes in mechanical prototype design and additive manufacturing technologies.

Vassil Atanassov received the B.Eng. degree (first class Hons.) in mechanical engineering from the University of Glasgow, Glasgow, U.K., in 2021 and the master's (*Cum Laude*) degree in robotics from the Delft University of Technology, Delft, The Netherlands, in 2023. He is currently working toward the Ph.D. degree in robotics with the Department of Engineering Science, University of Oxford, Oxford, U.K.

His research interests include model-based and data-driven control of legged robots.

Fabio Boekel received the B.Eng. degree in mechanical engineering in 2021 from the Delft University of Technology, Delft, The Netherlands, where he is currently working toward the M.Sc. degree in robotics.

His research interests include the design and control of legged robots.

Jens Kober (Senior Member, IEEE) received the Ph.D. degree in engineering from TU Darmstadt, Darmstadt, Germany, and the Max Planck Institute for Intelligent Systems, Stuttgart, Germany, in 2012.

He is currently an Associate Professor with the TU Delft, Delft, The Netherlands. He was a Postdoctoral scholar jointly with the CoR-Lab, Bielefeld University, Bielefeld, Germany, and with the Honda Research Institute Europe, Offenbach, Germany. His research interests include motor skill learning, (deep) reinforcement learning, imitation learning, interactive learning, and machine learning for control.

Dr. Kober, for his research, was the recipient of the annually awarded Georges Giralt Ph.D. Award for the best Ph.D. thesis in robotics in Europe, the 2018 IEEE RAS Early Academic Career Award, the 2022 RSS Early Career Award, and an ERC Starting grant.

Cosimo Della Santina (Senior Member, IEEE) received the Ph.D. degree in robotics from the University of Pisa, Pisa, Italy, in 2019.

He was a Visiting Ph.D. student and a Postdoctoral Researcher (2017–2019) with the Massachusetts Institute of Technology, Cambridge, MA, USA. Since 2020, he is with the German Aerospace Centre as an external Research Scientist. He is currently an Assistant Professor with the Department of Cognitive Robotics, Delft University of Technology, Delft, The Netherlands. His research interests include modeling and control, robot learning and their applications on soft robotics.